Occupancy Driven Buildings-to-grid Integration Framework for Large Commercial Buildings

Zhaoxuan Li[1], Bing Dong[2]*, Hannah Fontenot[3]

[1] University of Texas at San Antonio, Department of Mechanical Engineering
San Antonio, Texas, U.S.A
zhaoxuan.li@utsa.edu

[2] University of Texas at San Antonio, Department of Mechanical Engineering
San Antonio, Texas, U.S.A
bing.dong@utsa.edu

[3] University of Texas at San Antonio, Department of Mechanical Engineering
San Antonio, Texas, U.S.A
hannah.fontenot@my.utsa.edu

* Corresponding Author

ABSTRACT

This paper proposes and develops an occupancy-based control and optimization framework for reducing energy consumption and cost within the context of Buildings-to-Grid (BtG) integration. A mathematical framework of large-scale integration, control, and optimization of solar powered buildings with battery energy storage systems and the grid is proposed and demonstrated. Building MPC formulations are designed based on appropriately linearized large commercial building conditioning and battery system models. A high-level linearized grid distribution network is also developed via IEEE standard grid systems with 9 and 14 buses. The final decentralized utility-scale BtG integrations with battery storages, photovoltaics generations, different grid systems, building occupancy simulators, and building HVAC

systems are conceptually designed and simulated. The results show that the integrated system can save up to 26% of total costs from buildings-to-grid operations.

1. INTRODUCTION

Globally, buildings demand plays an important role in the challenge of growing energy consumption. Buildings account for more than one-third of the total primary energy supply (IEA 2013). With the significant increase of energy consumption in buildings, energy saving strategies have become priorities in building management and operations. The categories of building services and heating, ventilation, and air conditioning (HVAC) systems make up almost 50% of energy usages of buildings (Shaikh et al. 2014). Therefore, the development and implementation of effective control techniques for HVAC systems can be one solution to reduce building energy consumption. In particular, with the decreased costs of data processing, storage, and communication over recent years, smart controls that integrate HVACs, renewable generation resources, and distributed energy storages are becoming possible in a smart building environment.

Model Predictive Control (MPC) as one of the advanced techniques is extremely popular in building research comparing to other controlling approaches (Afram and Janabi-Sharifi 2014). MPC incorporates optimization along with system dynamics to achieve parallel goals of comfort regulation and energy saving. It uses a system model to predict the future states of the system and generates a control vector that minimizes a certain cost function over the prediction horizon in the presence of disturbances and constraints. Most MPCs use ubiquitous simulations of certain modeling to solve a computationally complex optimization problem in finite prediction time steps, so that control stabilities and multiple optimization goals can be achieved. An MPC optimization problem can be formulated in numerous ways, but can be presented using a nonlinear form in general as follows:

$$\min \sum_{k=0}^{k=N-1} c_i(\mathbf{x}_{t+k|t}, \mathbf{u}_{t+k|t}, \mathbf{w}_{t+k|t})$$

$$\text{s.t. } \mathbf{x}_{t+k+1|t} = \mathbf{f}(\mathbf{x}_{t+k|t}, \mathbf{u}_{t+k|t}, \mathbf{w}_{t+k|t})$$

$$\mathbf{y}_{t+k|t} = \mathbf{g}(\mathbf{x}_{t+k|t}, \mathbf{u}_{t+k|t}, \mathbf{w}_{t+k|t})$$

$$\mathbf{x}_{t+k|t} \in \mathbf{X}$$

$$\mathbf{u}_{t+k|t} \in \mathbf{U} \tag{1}$$

$$\mathbf{y}_{t+k|t} \in \mathbf{Y}$$

where $\mathbf{x}_{t+k|t}$ are the system states, $\mathbf{u}_{t+k|t}$ are the system control inputs, $\mathbf{w}_{t+k|t}$ are the system disturbances, $\mathbf{y}_{t+k|t}$ are the system outputs, $\mathbf{t}$ is the current control time step, $\mathbf{k}$ is the future predictive time step, $\mathbf{N}$ is the total time steps needing to be predicted and optimized in MPC, functions $\mathbf{f}$ and $\mathbf{g}$ are the system models, and system states, inputs, and outputs are constrained by $\mathbf{X}$, $\mathbf{U}$, and $\mathbf{Y}$ respectively.

Along with smart buildings, new grid policies are heavily promoted in the U.S. The U.S. government ˌs energy policies aim to create a secure supply of energy, keep energy costs low, and protect the environment by reducing consumption through increased energy efficiency, increased domestic production of conventional energy sources, and development of new sources of energy, particularly renewable energy and renewable fuels (Behrens 2013). There are many objectives which can be achieved in power grid control. One main objective, which is the interest of this study, is to manage power flow. Optimal power flow (OPF) management is an essential day-ahead operational planning tool widely used in research and industry. It aims to minimize a certain objective function (e.g., operation cost) while satisfying operational constraints on branch current and bus voltage. The conventional OPF problem can be stated in an abstract form, which is similar to building MPC, as follows:

$$\min \quad \mathbf{f(x,u)}$$
$$\text{s.t.} \quad \mathbf{g(x,u,w) = 0}$$
$$\mathbf{h(x,u,w) \leq H} \tag{2}$$
$$\mathbf{x \in X}$$
$$\mathbf{u \in U}$$

where $\mathbf{x}$ are the state variables (i.e., voltage magnitude and angle), $\mathbf{u}$ are the control inputs (i.e., generator active power and terminal voltage), $\mathbf{w}$ are the system disturbances (i.e., grid base power demand), $\mathbf{g}$ is the power flow model, $\mathbf{h}$ is the operational limit function (i.e., branch current and voltage magnitude), and system states and inputs are constrained by $\mathbf{X}$ and $\mathbf{U}$ respectively.

Based on the aforementioned review, there is a demand for an innovative and holistic approach for control design and system operation which allows multiple-system controls in the context of a large scale buildings-to-grid integration for cost and energy reductions. Several research gaps are present in the current research field: 1) lack of a holistic simulation framework for the integration of occupancy, buildings, renewable resources, and grid, 2) lack of advanced control strategy designed on a large scale for buildings and grid, 3) lack of coupling of realistic nonlinear plants and linear controller for multiple-component buildings-to-grid system, and 4) lack of coordination of control time step discrepancy between buildings and grid. This study aims to fill some of the research gaps in the current-state-of-the-art by: 1) Developing a new online occupancy predictor for control purposes to predict the occupancy at the building level; 2) Developing nonlinear building load and conditioning models which are capable of large scale simulation and control; 3) Developing nonlinear distributed energy resources which are able to be integrated into building controls; 4) Designing and developing a hierarchical building controller using appropriate linearization techniques to incorporate building occupancy predictions, nonlinear system plants, and building comfort regulations; 5) Designing and developing a high level control and simulation framework between buildings and grid with system-level objectives and constraints to address the operation time-scale discrepancy and the large-scale computational cost. The remainder of this study is

structured as follows: Section 2 introduces the system models used in this study; Section 3 introduces the Model Predictive Control (MPC) of the buildings and grid; and Section 4 illustrates the simulation results.

2. System Models

2.1 Building Occupancy Model

A Markov model is used as developed earlier in previous study (Li and Dong 2018). Given n_{ij} pairs of the transitional states, observed as $\{s_i, s_j\}$, of all pairs of the transitional states $\{s_i, s_l\}$ that belong to the training data, the transitional probability is estimated as

$$\hat{p}_{ij} = \frac{n_{ij} + \alpha}{\sum\limits_{l=1}^{k}(n_{ij} + \alpha)} \tag{3}$$

where α is a smoothing factor and k is the maximum number of occupancy states observed. A properly defined smoothing factor could enforce the likelihood of occupancy changes during the dramatic increase of occupancy presence at the morning ramp-up, and dramatic decrease of occupancy presence at the evening ramp-down. The Markov occupancy model is going to be integrated into a rolling window MPC. Assuming a building MPC is rolling at a 15-minute resolution, there will be a total of 96 sets of transition probabilities which need to be updated for a day-ahead MPC optimization. For each set of time inhomogeneous transitional probabilities, they are estimated within an optimal window before each of the predicted time steps. The period of the optimal window is decided by the changing point of the occupancy rate based on a daily profile of the historical occupancy. To overcome the uncertainties from the limited training window, a modified bootstrap sampling strategy is used as follows:

1) Randomly sample nine days from the training data and apply Eq. (3) to get one bootstrap set of transitional probabilities;
2) Resample ten times using the procedure above;
3) Calculate the average values of the ten bootstrap sets.

The selection of training data set for the model relies on the occupancy change-point analysis. Since the authors design the model for a rolling MPC, the daily profile is constantly updated. Thus a visual identification of change points is not adaptive. Let $D = \{d_1, ..., d_{96 \times z}\}$ represent all historical occupancy before prediction day. Here, historical information contains all the working days z that are updated for MPC. A discrete profile of the occupancy rates in daily scale is generated by

$$P(i) = \frac{\sum\limits_{j=1}^{z}(\lambda^{z-j} d_{(j-1) \times 96 + i})}{z} \tag{4}$$

where d is the chain state which is a binary occupancy containing only 0 and 1, i is the time step of the daily profile where $1 < i < 96$ if the occupancy data is in 15-min scale, and λ is an exponential forgetting

factor, which is below 1. The forgetting factor reduces the influence from the too-old occupancy information.

The change-point detection algorithm uses relative density-ratio estimation with the Pearson divergence scoring the possible change points of the daily profile $P(i)$. For a data set m sampled from the daily profile D, the divergence score is defined as follows:

$$\int P_\beta(m)\left[\frac{P(D)}{P_\beta(m)}-1\right]^2 d(m)+\int P(D)\left[\frac{P_\beta(m)}{P(D)}-1\right]^2 d(D) \tag{5}$$

where $P_\beta(m)=\beta P(D)+(1-\beta)P(m)$, P is the probability density function of the corresponding data set, and the factor β is a weight factor which is 0.5 to put equal weight on each of the distributions. For the example of Figure 2, the day file as the sample D contains 96 occupancy rates in 15-minute resolution. The data set m is sampled using a sliding window size of 12 (3 hour data). The sliding continues forward until end of the day and then resamples backward again. A symmetric score is calculated by the summation of forward sliding and backward sliding scores using Eq. (5). The MATLAB toolbox developed by Liu is used in this study (Liu et al. 2013).

2.2 Building Thermal Model

The total electricity demands of commercial buildings are mainly comprised of two parts: base power demands and controllable power demands. Lighting, electrical equipment, and office appliances are associated with base demands, which can be modelled and predicted by operation schedules. In contrast, HVAC systems are controllable building components whose demands may be altered by adjusting building indoor temperature setpoints. The optimal HVAC demand can be estimated through the control of the building physics model, and specifically, the thermal resistance and capacitance (RC) network. A super zone model is proposed for the convenience of the large scale simulation, a 2R-1C thermal network model. It only has two temperature states, namely, building zonal temperature T_{zone} and building wall structure temperature T_{wall} for each building. The thermodynamics of this thermal network model are expressed as:

$$C\dot{T} \qquad \frac{-T_{wall}}{R_2}+\frac{T_{zone}-T_{wall}}{R_1}+Q_{sol}$$
$$C_{zone}\dot{T} \qquad \frac{-T_{zone}}{R_1}+\frac{T_{amb}-T_{zone}}{R_{win}}+Q_{int}+Q_{hvac} \tag{6}$$

where R_1, R_2, and R_{win} are the aggregated thermal resistances of the exterior structure, interior structure, and window; C_{zone} and C are the aggregated thermal capacitances of the zone and walls˒ structure; T_{amb}, T_{wall}, and T_{zone} are the ambient exterior temperature, the walls˒ structure temperature, and the aggregated zone temperature; and Q_{sol}, Q_{int}, and Q_{hvac} are the solar disturbance heat gain, the internal heat gain from the miscellaneous power consumption, and the HVAC load from the conditioning power consumption.

Larger commercial buildings have more systems for building conditioning, normally including cooling towers, Air Handling Units (AHUs), electricity chillers and more. The whole system has two loops: water loop and air loop. In the water-loop system, a centralized chilled water generation system produces the required cooling energy. It is assumed that chillers could be operated at various conditions to meet the partial cooling demands. In the air-loop system, subsystems known as AHUs transfer energy from distributed chilled water into localized air flows. These air flows are transported to building spaces, delivering cooling energy where required. The AHUs recirculate return air at temperature T_{ra} from building spaces and mix it with fresh outside air at temperature T_{oa} to produce a mixed air temperature of T_{ma}. The ratio of return air flow to outside air flow is controlled by dampers located inside the AHUs. The mixed air is cooled by a cooling coil that transfers cooling energy from the chilled water that is generated or stored by the water-loop system. The air temperature of the downstream air flow passing by the cooling coil is monitored as supply air temperature to the building zones, T_{sa}. T_{sa} is usually maintained within a certain range. The state space equation integrating AHUs and the thermal RC network of building l is expressed as follows:

$$\dot{\mathbf{g}}_{\mathbf{b}}^{\mathbf{l}} = \mathbf{A}_{\mathbf{g}}^{\mathbf{l}}\mathbf{g}_{\mathbf{b}}^{\mathbf{l}} + \mathbf{B}_{\mathbf{u}}^{\mathbf{l}}\mathbf{u}_{\mathbf{b}}^{\mathbf{l}} + \mathbf{B}_{\mathbf{w}}^{\mathbf{l}}\mathbf{w}_{\mathbf{g}}^{\mathbf{l}} + \mathbf{B}_{\phi}^{\mathbf{l}}\phi(\mathbf{g}_{\mathbf{b}}^{\mathbf{l}},\mathbf{u}_{\mathbf{b}}^{\mathbf{l}},\mathbf{w}_{\mathbf{g}}^{\mathbf{l}}) \tag{7}$$

where $\mathbf{g}_{\mathbf{b}}^{\mathbf{l}} = \begin{bmatrix} T_{wall} \\ T_{zone} \\ T_{sa} \end{bmatrix}$ are building temperature states containing T_{wall} (the structure temperature), T_{zone} (the zone temperature), and T_{sa} (the AHU supply air temperature); $\mathbf{u}_{\mathbf{b}}^{\mathbf{l}} = \begin{bmatrix} f_{air} \\ f_{water} \end{bmatrix}$ are the building conditioning control inputs containing control variables f_{air} (the AHU air flow) and f_{water} (the chiller water flow); $\mathbf{w}_{\mathbf{b}}^{\mathbf{l}} = \begin{bmatrix} T_{amb} \\ Q_{sol} \\ Q_{int} \end{bmatrix}$ are the building disturbances which are the same as in Eq. (6); $\mathbf{A}_{\mathbf{g}}^{\mathbf{l}} = \begin{bmatrix} a_{11} & a_{12} & 0 \\ a_{21} & a_{22} & 0 \\ 0 & 0 & 0 \end{bmatrix}$ is the coefficient matrix of the building states containing parameters $a_{11} = -\dfrac{R_1+R_2}{CR_1R_2}$, $a_{21} = -\dfrac{1}{CR_1}$, $a_{21} = \dfrac{1}{C_{zone}R_1}$, $a_{22} = -\dfrac{R_1+R_{win}}{C_{zone}R_1R_{win}}$ where the symbols are the same as in Eq. (6); $\mathbf{B}_{\mathbf{u}}^{\mathbf{l}} = \begin{bmatrix} 0 & 0 \\ 0 & 0 \\ 0 & b \end{bmatrix}$ is the coefficient matrix of the control inputs containing parameters $b = -\dfrac{\rho_w C_w \Delta T_w}{\rho_a C_a V_{AHU}}$ where ρ_w is the water density, ρ_a is the air density, C_w is the water specific heat, C_a is the air specific heat, ΔT_w is the temperature difference between the inlet and outlet chiller water, and V_{AHU} is the AHU volume; $\mathbf{B}_{\mathbf{wb}}^{\mathbf{l}} = \begin{bmatrix} c_{11} & c_{12} & 0 \\ c_{21} & 0 & c_{23} \\ 0 & 0 & 0 \end{bmatrix}$ is the coefficient matrix of the building disturbances containing parameters $c_{11} = \dfrac{1}{CR_2}$, $c_{12} = \dfrac{1}{C}$, $c_{12} = \dfrac{1}{C_{zone}R_{win}}$, $c_{23} = \dfrac{1}{C_{zone}}$ where the

symbols are the same as in Eq. (6); $\mathbf{B}_\phi^1 = \begin{bmatrix} 0 & 0 & 0 \\ d_{21} & d_{22} & 0 \\ d_{31} & d_{32} & d_{33} \end{bmatrix}$ is the coefficient matrix of the nonlinear part

containing parameters $d_{21} = -\dfrac{\rho_a C_a}{C_{zone}}$, $d_{22} = \dfrac{\rho_a C_a}{C_{zone}}$, $d_{31} = \dfrac{0.3}{C_{zone}}$, $d_{32} = -\dfrac{1}{V_{AHU}}$, $d_{33} = -\dfrac{0.7}{C_{zone}}$ where the symbols

are the same as in Eq. (6); Note that the mixed air is designed to mix 70% of the outdoor air and 30%

indoor return air; and $\phi(\mathbf{g}_\mathbf{b}^1, \mathbf{u}_\mathbf{b}^1, \mathbf{w}_\mathbf{g}^1) = \begin{bmatrix} f_{air} T_{wall} \\ f_{air} T_{zone} \\ f_{air} T_{amb} \end{bmatrix}$ is the nonlinear part where variable definitions are the

same as previously mentioned.

For the water loop, the chillers consume electricity to extract energy from the coolant water flows. The power consumed by the coils is expressed as

$$P_{chiller} = f(n, Q_{ref}, Q_{AHU}, T_{cond}, T_{chw}) \tag{8}$$

where Q_{ref} is the reference chiller consumption when the chiller is on at full conditioning, n is the number of chillers operated, Q_{AHU} is the AHU power demand from the air-loop side, T_{cond} is the condenser discharge temperature of the cooling tower, and T_{chw} is the chiller supply temperature. An equivalent regression fitting form is

$$P_{chiller} = \frac{n Q_{ref} f_{EIR} f_{PLR}}{COP \cdot f_{CCF}} \tag{9}$$

where $f_{CCF} = a_1 + a_2 T_{cond} + a_3 T_{cond}^2 + a_4 T_{chw} + a_5 T_{chw}^2 + a_6 T_{cond} T_{chw}$ is the Cooling Capacity Factor (CCF) function, $f_{EIR} = b_1 + b_2 T_{cond} + b_3 T_{cond}^2 + b_4 T_{chw} + b_5 T_{chw}^2 + b_6 T_{cond} T_{chw}$ is the Energy Input Ratio (EIR) function, $f_{PLR} = c_1 + c_2 T_{cond} + c_3 T_{cond}^2 + c_4 C_{PLR} + c_5 C_{PLR}^2 + c_6 T_{cond} C_{PLR} + c_7 C_{PLR}^3$ is the Patrial Load Ration (PLR) function with $C_{PLR} = \dfrac{Q_{AHU}}{Q_{ref}}$, and COP is a constant parameter defined as coefficient of performance.

2.3 Distributed Energy Resources

Electrochemical batteries are of great importance for future smart buildings because the chemical energy stored inside them can be converted into electrical energy and delivered to building systems whenever and wherever electricity energy is needed. A linearized battery model can be used in large scale simulation as:

$$Q_o \frac{d}{dt} SOC(t) = \eta P(t) \tag{10}$$

where SOC is the state of battery charging and discharging, Q_o is the nominal battery capacity, η is the charging and discharging efficiency, and P is the charging and discharging power.

Another popular distributed energy resource for smart buildings is the Photovoltaic (PV) system. Machine learning, ANN, is used to predict PV generation. Feed Forward Neural Network (FFNN) of ANN is used in this study. The authors explore both single hidden layer and double hidden layer FFNN. However, the structure of double hidden

layer is abandoned due to an overfitting problem. This observation matches conclusions regarding hidden layer selection by the authors' previous studies (Dong et al. 2016), and deep learning may be one solution to the problem which is beyond the topics of this study. A single layer model to approximate the PV production in FFNN is expressed as

$$y = \sum_{j=1}^{N} w_j \varphi_j [\sum_{i=1}^{M} w_{ij} x_i + w_{io}] + w_{jo} \tag{11}$$

where w is the weight for input layer, hidden layer, and output layer indexed by i, j, and o, x is the training input, y is the training output, N represents the total number of hidden units, M represents the total number of inputs, and φ represents the learning function for each hidden unit.

2.4 Grid Model

Several models of grid systems exist, each with different accuracy and computational complexity (Zimmerman, et al. 2011; Low et al. 2014). Considering a standard IEEE case, the total electrical power injection S_k into bus k can be expressed as

$$S_k = P_k - jQ_k \tag{12}$$

where P_k is the active power injection and Q_k is the reactive power injection. It is also noticed that the power variable is a complex number. Physical considerations dictate the following complex parameter for the transmission line connecting bus k and bus j

$$Y_{kj} = g_{kj} - b_{kj} i \tag{13}$$

where Y_{kj} is the admittance of the transmission line connecting bus node k and bus node j, g_{kj} is the conductance of the transmission line, b_{kj} is the susceptance of the transmission line, and i is the imaginary unit. The real and reactive power injections into bus k become power flows on the transmission lines. Using Ohm ̦s Law, the real and reactive power flows on the line connecting buses k and j are expressed as

$$P_{kj} = V_k^2 g_{kj} - V_k V_j [g_{kj} \cos(\theta_k - \theta_j) - b_{kj} \sin(\theta_k - \theta_j)] \tag{14}$$
$$Q_{kj} = V_k^2 b_{kj} - V_k V_j [g_{kj} \sin(\theta_k - \theta_j) + b_{kj} \cos(\theta_k - \theta_j)]$$

where $V_k, V_j, \theta_k, \theta_j$ are the voltage magnitudes (kV) and voltage angles of buses k and j respectively. However, accurate power flow equations in Eq. (14) are computationally challenging in the scope of large-scale BtG integration, especially given the nonlinear formulations. A simplified power flow model can be alternatively formulated under reasonable assumptions that tend to hold in practice (Giannakis et al. 2013). These assumptions enable the linearization of Eq. (14) as

$$P_{kj} = V_o^2 b_{kj} (\theta_k - \theta_j) \tag{15}$$

where V_o is the base voltage magnitude (kV). The parameter V_o can be further eliminated by scaling it to a dimensionless per unit (p.u.) quantity so that $|V_o| \approx 1 p.u.$.

The generators connected to the grid are normally synchronous machines with rotors that spin at synchronous speed. The dynamics of the mechanical power transferring to electricity power by the generators are modeled by the rotational counterpart of Newton ̦s law

$$J\ddot{\theta} \qquad \cdot T^e \qquad (16)$$

where θ is the rotor voltage angle which rotates at a certain frequency, J is the moment of inertia, T^m is the mechanical torque input to the generator from the turbine, and T^e is the electrical torque on the generator rotor. The electrical torque corresponds to the electrical power that the generator provides. This electrical power serves any load attached to the generator bus or is converted to power flows on the lines leaving the generator bus. In Eq. (16), the first derivative $\dot{\theta}$ is the angular frequency ω. The left-hand side of Eq. (16) is typically augmented by a damping torque that is proportional to $\dot{\theta}$. The nominal value of the angular frequency corresponds to the electrical frequency of 60 Hz that is used in North America ˌs grid. Supposing that the angular frequency remains close to its nominal value, the mechanical and electrical torques in Eq. (16) are converted to powers by multiplying with the nominal angular frequency, which results in the *swing equation* for bus k

$$M_k\ddot{\theta} \qquad \cdot \qquad P_k^e - \sum_{j=1}^{n} P_{kj} \qquad (17)$$

where n is the number of buses, θ_k is the bus voltage angle, M_k is the inertia coefficient, D_k is the damping coefficient, P_k^m is the mechanical power input to generator, P_k^e is the electricity load demand at bus k, P_{kj} is the power flow from bus k to bus j, $\sum_{j=1}^{n} P_{kj}$ is the cumulative power flow over line (k,j), and n is the number of buses in the network. The power flow P_{kj} of Eq. (17) is given by

$$P_{kj} = b_{kj}(\theta_k - \theta_j) \qquad (18)$$

where $P_{kj} = 0$ if there is no line connecting buses k and j. The electricity load P_k^e at the k th bus of Eq. (17) can be decomposed into three components as

$$P_k^e = E_k\dot{\theta} \qquad \sum_{l=1}^{L} P_{\{k,l\}}^b \qquad (19)$$

where $E_k\dot{\theta}$ is the frequency-sensitive uncontrollable load, P_k^i is the frequency-insensitive load, P^b is the individual building power load, and $\sum_{l=1}^{L} P_{\{k,l\}}^b$ is the cumulative power demand from the buildings that are connected to the k th bus; the total number of connected buildings is L.

The individual building power load in Eq. (19) is defined as

$$P^b = P_{hvac} + P_{misc} \qquad (20)$$

where P_{hvac} is the HVAC load that can participate in frequency regulation, and P_{misc} represents the miscellaneous load with no potential to contribute to frequency regulation in this study.

By combining Eq. (17)-(20), the authors obtain a governing equation by letting $\dot{\theta}$ for the grid system as

$$M_k\ddot{\theta} \qquad + E_k)\omega_k + P_k^m + \sum_{j=1}^{n} b_{kj}(\theta_k - \theta_j) - P_k^i - \sum_{l=1}^{L} (P_{hvac}^l + P_{misc}^l) \qquad (21)$$

A linear state-space representation of the grid system can be derived based on Eq. (21) as

$$\mathbf{A_e}\dot{\mathbf{x}} \qquad + \mathbf{A_{ub}u_b} + \mathbf{B_m u_m} + \mathbf{B_{wg} w_g} \qquad (22)$$

3. System Controls

3.1 Building Control

By assuming building states (wall and zone temperatures) in Eq. (7) as the zone setpoint, state space equations of large commercial buildings can be linearized as

$$\dot{\mathbf{g}_b^l} = \mathbf{A}_g^l \mathbf{g}_b^l + \mathbf{\Phi}_u^l \mathbf{u}_b^l + \mathbf{B}_w^l \mathbf{w}_g^l \tag{23}$$

where

- $\mathbf{g}_b^l$, $\mathbf{u}_b^l$, $\mathbf{w}_g^l$, $\mathbf{A}_g^l$, and $\mathbf{B}_w^l$ are all the same as in Eq. (7); and

- $\mathbf{\Phi}_u^l = \begin{bmatrix} 0 & 0 \\ (d_{21}+d_{22})S_t & 0 \\ (d_{31}+d_{32})S_t + d_{33}T_{amb} & b \end{bmatrix}$ is the linearized coefficient matrix of the control inputs; Note that S_t and T_{amb} are the setpoint and ambient outdoor air temperature at the time step t while other parameters definitions are the same as Eq. (7).

Therefore, the large commercial building MPC can be formulated as

$$\min_{U_b} \int_0^t (\mathbf{c}_{AHU}^T \mathbf{u}_b^l) dt$$

$$\text{s.t.} \quad \dot{\mathbf{g}_b^l} = \mathbf{A}_g^l \mathbf{g}_b^l + \mathbf{\Phi}_u^l \mathbf{u}_b^l + \mathbf{B}_w^l \mathbf{w}_g^l$$

$$\mathbf{g}_b^{min} \leq \mathbf{g}_b^l \leq \mathbf{g}_b^{max} + \mathbf{\varepsilon}_{ub}(O)$$

$$\mathbf{g}_b^{min} \leq \mathbf{g}_b^l \leq \mathbf{g}_b^{max}$$

$$\mathbf{u}_b^{min} \leq \mathbf{u}_b^l \leq \mathbf{u}_b^{max} \tag{24}$$

where $\mathbf{c}_{AHU}$ refers to the cost of building AHU power consumption based on the grid price (\$/kWh) while other states and parameters are defined similar to Eq. (7) and Eq. (23). The authors introduce an occupancy-based slack relaxation on the building states constraints of Eq. (24). The occupancy information such as presence and absence are simulated and predicted based on the occupancy model in Section 2.1. The model is designed to focus on the occupancy status at the whole building level. For example, the occupancy model predicts the lunch break as absence during certain time periods if the aggregated training data show a majority of the people leaving the offices for lunch. Hence, the upper bounds on indoor temperature increases from $\mathbf{x}_b^{max}$ to $\mathbf{x}_b^{max} + \mathbf{\varepsilon}_{ub}(O)$ during cooling condition. Function $\mathbf{\varepsilon}_{ub}(O)$ is the occupancy-based slack relaxation function, and O is the binary occupancy state at optimized time step t. The relaxation function in Eq. (24) is defined as

$$\varepsilon_{ub}(O(t)) = \begin{cases} \Delta T & if \quad 0 \leq \Gamma(O) < 1 \\ \min\{\Delta T, \mathbf{x}_b(t-1) - \mathbf{x}_b^{max}(t-1) - \mathbf{\varepsilon}_{ub}(O(t-1))\} & if \quad \Gamma(O) > 1 \\ 0 & if \quad \Gamma(O) = 1 \end{cases} \tag{25}$$

where ΔT is the constraint adjustment threshold for building states (1-2 °C), conditional function Γ is defined as $\Gamma(O) = O + \max\{0, \mathbf{x}_b(t-1) - \mathbf{x}_b^{max}(t-1) - \mathbf{\varepsilon}_{ub}(O(t-1))\}$ with $\mathbf{x}_b$ as building states vector and $\mathbf{x}_b^{max}$

as the predefined upper bound of building states. This empirically derived relaxation formulation is designed to balance the feasibility of the numerical solver and the savings of the optimal solution.

3.2 Grid Control

The grid MPC optimizes the power generation costs as well as the cost of frequency deviations. It is assumed that each generator has variable and fixed costs of production while transmission loss is negligible. Simplified cost optimization is developed without considerations of the no-load operation, startup or shutdown costs, and ramping constraints. Letting $\mathbf{u_m}$ in Eq. (22) be $\mathbf{u_m} = \mathbf{\bar{u}_m} + \Delta\mathbf{u_m}$ where $\Delta\mathbf{u_m}$ is the additional adjustments on the mechanical power setpoints $\mathbf{\bar{u}_m}$, the total cost function of the generators takes the form of

$$\int_0^t (\mathbf{\bar{u}_m}^T \mathbf{A_{\bar{u}}} \mathbf{\bar{u}_m} + \mathbf{B_{\bar{u}}^T} \mathbf{\bar{u}_m} + c\Delta\mathbf{u_m^T} \mathbf{A_{\Delta u}} \Delta\mathbf{u_m} + c\mathbf{B_{\Delta u}^T} \Delta\mathbf{u_m} + \mathbf{x_g}^T \mathbf{F_\omega} \mathbf{x_g})dt \tag{26}$$

where $\mathbf{\bar{u}_m} = \begin{bmatrix} \bar{u}_1 \\ \vdots \\ \bar{u}_{n_g} \end{bmatrix}$, $\mathbf{A_{\bar{u}}} = \begin{bmatrix} a_1 & & \\ & \ddots & \\ & & a_{n_g} \end{bmatrix}$ has units of \$/MW²h, and $\mathbf{B_{\bar{u}}} = \begin{bmatrix} b_1 \\ \vdots \\ b_{n_g} \end{bmatrix}$ has units of \$/MWh, $\Delta\mathbf{u_m}$, $\mathbf{A_{\Delta u}}$, $\mathbf{B_{\Delta u}}$ are all defined similar as $\mathbf{\bar{u}_m}$, $\mathbf{A_{\bar{u}}}$, and $\mathbf{B_{\bar{u}}}$, $\mathbf{x_g}$ is the grid state in Eq. (22), c is the penalty factor on generators adjustments, and $\mathbf{F_\omega} = \begin{bmatrix} 0 & & & & \\ & f_g & & & \\ & & \ddots & & \\ & & & 0 & \\ & & & & f_g \end{bmatrix}_{2n \times 2n}$ is a diagonal matrix with the constant frequency deviation penalty f_g for frequency ω of $\mathbf{x_g}$.

The canonical linear form of the grid-only MPC during the prediction horizon $[0,t]$ combining Eq. (22) and Eq. (26) is written as

$$\min_{U_b} \int_0^t (\mathbf{\bar{u}_m}^T \mathbf{A_{\bar{u}}} \mathbf{\bar{u}_m} + \mathbf{B_{\bar{u}}^T} \mathbf{\bar{u}_m} + c\Delta\mathbf{u_m^T} \mathbf{A_{\Delta u}} \Delta\mathbf{u_m} + c\mathbf{B_{\Delta u}^T} \Delta\mathbf{u_m} + \mathbf{x_g}^T \mathbf{F_\omega} \mathbf{x_g})dt$$

$$\text{s.t.} \quad \mathbf{A_e}\dot{} \qquad + \mathbf{A_{ub}}\mathbf{u_b} + \mathbf{B_m}\mathbf{u_m} + \mathbf{B_{wg}}\mathbf{W_g}$$

$$\Delta\mathbf{u_m^{min}} \leq \Delta\mathbf{u_m} \leq \Delta\mathbf{u_m^{max}}$$

$$\mathbf{\bar{u}_m^{min}} \leq \mathbf{\bar{u}_m} \leq \mathbf{\bar{u}_m^{max}}$$

$$\mathbf{x_g^{min}} \leq \mathbf{x_g} \leq \mathbf{x_g^{max}} \tag{27}$$

$$\mathbf{A_f}\mathbf{x_g} \leq \mathbf{F_{max}}$$

where $\mathbf{u_b}$ are building HVAC loads and $\Delta\mathbf{u_b^{min}}, \Delta\mathbf{u_b^{max}}, \mathbf{\bar{u}_b^{min}}, \mathbf{\bar{u}_b^{max}}, \mathbf{x_g^{min}}, \mathbf{x_g^{max}}$ are the minimum and maximum constraints for the corresponding building control variable and grid system states. Other parameter notations are the same as in Eq. (26).

3.3 Buildings-to-Grid Control

The integration of the building MPC and the grid MPC from Section 3.1 and Section 3.2 can formulate a decentralized framework that optimizes the cost of the buildings and the grid simultaneously. Given the case of large-scale BtG MPC, the authors first limit the forecasting window of MPC at 15-minute ahead prediction for each rolling step. The rolling step is 10 seconds to match the normal grid operation. During each period of 10 seconds, the BtG MPC control trajectories are calculated for both building and grid at 15 minutes ahead. However, it is not necessary to optimize the building control at 10-second interval for each MPC due to the slow responses of the building thermal states. The authors propose a two-level MPC that addresses the issues of the operational time discrepancy between buildings and grid to reduce the computational complexity, where the control variables are described next and are depicted in Figure 1.

The two level BtG MPC framework is described as follows:

1)   Level 1: The first level of BtG MPC is only used exactly every 5 mins. In other words, only the rolling steps that occur every 5 mins uses level-one MPC to optimize three control variables of Eq. (24) and Eq. (27) for the next 15 mins: the building HVAC power $\mathbf{u_b}$, the mechanical power setpoints $\mathbf{\bar{u}_m}$ for generators, and the adjustments of the mechanical power setpoints $\mathbf{\Delta u_m}$. For the example in Figure 1, one generator ‚s setpoint $\bar{u}_m$, one generator ‚s adjustment Δu_m, and one building HVAC power u_b are going to be optimized simultaneously every 5 mins.

2)   Level 2: If the rolling MPC is continuing in-between every 5 mins, a level-two MPC is designed based on the optimized building HVAC power $\mathbf{u_b}$ and the optimized mechanical power setpoints $\mathbf{\bar{u}_m}$ from the previous level-one MPC. Only the adjustments are updated and optimized every 10 secs. Using the example in Figure 1 again, the rolling steps from 10 secs to 4 mins and 50 secs have constant $\bar{u}_m$ and Δu_m at all the times for each rolling MPC while $\bar{u}_m$ and u_b are optimized during each MPC. The values of and are optimized values from the first level-one MPC.

4. Simulation Results

A prototype commercial building from previous study (McFadden et al. 2015) is used here to randomly generate the building clusters. Random factors drawn from a uniform distribution are used to randomize the building parameters for a large-scale simulation of 1000 buildings. The internal load is determined by the ASHRAE standard definitions on the lighting power density and equipment power density per meter square. For the building HVAC system, one week of summer weather data collected during the year of 2014 by a local weather station at San Antonio are used. A night setback strategy for non-office hours is used for the HVAC baseline simulation. Office hours are defined from 7:30 am to 8:00 pm, while early start-up of the system is set from 7:00 am to 7:30 am. The setpoint for office hours is 74°F (23.33°C) with 1°F deadband (23.33°C$\pm$0.55). After all parameters of the buildings are randomized, the physics models are obtained as detailed in Section 3.1. The chillers used in the section are a reference model developed in

(Monfet et al. 2011). The system has 900 tons of cooling capacity and 28 days of calibration data with estimated coefficient of performance of 5.29. The detailed operation characteristics are described in (Monfet et al. 2011). The distributed energy resources are randomized based on estimated building power peak demand that can participate in grid regulation. An empirical rule of randomized 10%-20% peak demand is used to determine the PV peak sizing while battery size is randomized as 200%-250% of PV sizing. To demonstrate the improvements of the control designed in this study, PIDs are used to be compared as baselines. The complete occupancy-based building-battery-PV MPC (OBBPMPC) is used to integrate all system models including air conditioning, batteries, occupancy, and PVs. The performances of controls of supply air temperature of AHU, zone air temperature of building, and power consumption of the building for cooling are presented in Figure 2. Blue lines represent the mean value of one example building cluster (500 buildings). Pink areas represent deviations of the simulated values of the same example building cluster. Grid control based on MPC, or GMPC, is used for integrated buildings-to-grid control. Simulation of grid is performed on IEEE Case 14 system. The operation costs and reductions comparing the baseline to using integrated buildings-to-grid (BtG) control are presented in Table 1.
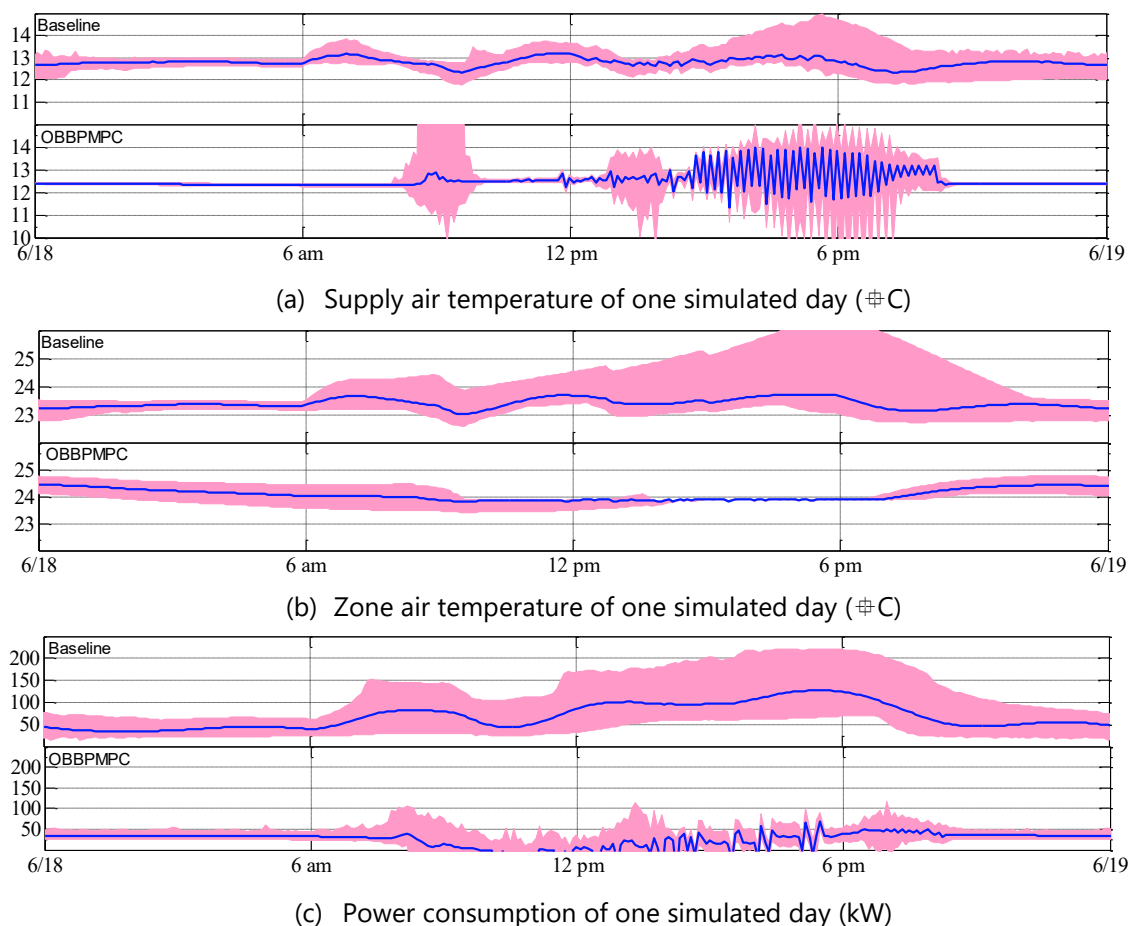

(a) Supply air temperature of one simulated day (⊕C)

(b) Zone air temperature of one simulated day (⊕C)

(c) Power consumption of one simulated day (kW)

Figure 1: MPCs with time discrepancy in a decentralized framework.

Table 1: Operation costs comparison

BtG Controls	Frequency Penalty (1000$)	Reduction	Generation Cost (1000$)	Reduction	Total BtG Cost (1000$)	Reduction
Baseline + GMPC	3.12	-	663.39	-	1117.77	-
OBBPMPC+ GMPC	2.84	8.97%	508.96	23.27%	818.80	26.74%

5. CONCLUSIONS

This study develops and demonstrates an innovative control framework that facilitates the interaction of building load controls with power grid generations, leading to a holistic Buildings-to-Grid integration. The simulation framework explicitly includes all detailed physics models of the occupancy, the building nonlinear conditionings, the distributed energy resources, and the grid systems at community scale for high-level optimization. Occupancy-based model predictive control for building clusters is developed for reducing total energy costs and maintaining thermal comfort. Distributed energy resources are integrated in the building control to reduce the peak demand and baseline energy usage. Optimal power flow problems for frequency control are explored for standard power systems. The simulations are performed using real data collected from local weather stations, ground truth prices, and onsite occupancy information to mimic practical cases. Simulations show significant reduction for electricity generation cost up to 23%, and total buildings-to-grid cost up to 26%. Future research should focus on a centralized or distributed control platform. It should co-optimize more complex systems of buildings and grids, high-order thermal networks such as EnergyPlus, and nonlinear grid models such as AC grid system, to achieve multi-objective optimization in the BtG integration.

REFERENCES

Afram, A. and Janabi-Sharifi, F. (2014). Theory and applications of HVAC control systems– A review of model predictive control (MPC). *Building and Environment*, 72: 343-355.

Behrens C.E. (2013). Energy policy: 113th congress issues.

Dong, B., Li, Z., Rahman, S.M. & Vega, R. (2016). A hybrid model approach for forecasting future residential electricity consumption. *Energy and Buildings*, 117: 341-351.

Giannakis, G.B., Kekatos, V., Gatsis, N., Kim, S.J., Zhu, H. & Wollenberg, B.F. (2013). Monitoring and optimization for power grid: A signal processing perspective. *IEEE Signal Processing Magazine*, 30(5): 107-128.

International Energy Agency. (2013). Transition to Sustainable Buildings: Strategies and Opportunities to 2050.

Li, Z. & Dong, B. (2018). Short term predictions of occupancy in commercial buildings—Performance analysis for stochastic models and machine learning approaches. *Energy and Buildings*, 158: 268-281.

Liu, S., Yamada, M., Collier, N. & Sugiyama, M. (2013). Change-point detection in time-series data by relative density-ratio estimation. *Neural Networks*, 43: 72-83.

Low, S.H. (2014). Convex relaxation of optimal power flow—Part I: Formulations and equivalence. *IEEE Transactions on Control of Network Systems*, 1(1): 15-27.

McFadden, G., Li, Z. & Rolando Vega PhD, P.E. (2015). HVAC Load Forecasting Using LIDAR Data and Physics-Based Models. *ASHRAE Transactions*, 121.

Monfet, D. & Zmeureanu, R. (2011). Identification of the electric chiller model for the EnergyPlus program using monitored data in an existing cooling plant. In *Proceedings of the international IBPSA conference*. Sidney, Australia: International Building Performance Simulation Association.

Shaikh, P.H., Nor, N.B.M., Nallagownden, P., Elamvazuthi, I. & Ibrahim, T. (2014). A review on optimized control systems for building energy and comfort management of smart sustainable buildings. *Renewable and Sustainable Energy Reviews*, 34, 409-429.

Zimmerman, R.D., Murillo-Sánchez, C.E. & Thomas, R.J. (2011). MATPOWER: Steady-state operations, planning, and analysis tools for power systems research and education. *IEEE Transactions on power systems*, 26(1): 12-19.

ACKNOWLEDGEMENT